First principles simulations on migration paths of oxygen interstitials in MgAl2O4

Alexander Platonenko, Denis Gryaznov, Yuri F. Zhukovskii, Eugene A. Kotomin

Institute of Solid State Physics, University of Latvia, 8 Kengaraga, Riga LV-1063, Latvia

ABSTRACT

Thermal stability of the primary electronic defects – *F* type centers – in oxide materials is controlled by their recombination with much more mobile complementary defects – interstitial oxygen ions. Thus, study of interstitial ions migration is of a key importance for prediction of radiation damage in oxides. In this study, several possible migration trajectories for neutral and charged interstitial oxygen ions were calculated in $MgAl_2O_4$ spinel using the first principles calculations of the atomic and electronic structure. The lowest energy barriers are ~1.0 - 1.1 eV and 0.8 eV, respectively. The effective atomic charges, charge redistribution, bond lengths are analyzed in detail.

Keywords:

Radiation defects, Magnesium-aluminium spinel, interstitial oxygen, diffusion, first principles calculations

1. Introduction

Several radiation-resistant binary and ternary oxides (MgO, Al_2O_3, $MgAl_2O_4$) are considered as perspective candidates for the diagnostics/optical windows in fusion devises [1-3]. As is known, accumulation of radiation-induced defects affects optical and other properties of optical components. Thus, understanding of the defect stability and recombination becomes very important issue. It was suggested [4,5] that $MgAl_2O_4$ crystalline structure exhibits a very high tolerance to irradiation with fast neutrons due to efficient recombination of primary Frenkel defects – the *F* type centers (oxygen vacancies with trapped electrons) and complementary interstitial oxygen ions, O_i. It is well known also that in most ionic solids, including alkali halides [6,7] and binary oxides [8,9], anion interstitials are much more mobile than the *F* centers and thus control their recombination rate and defect concentrations. There were several experimental [3,5,10] and theoretical first principles [11] studies of radiation defects in $MgAl_2O_4$ mostly focused on the electronic centers, whereas O_i interstitials are studied very poorly. Only a few theoretical studies were performed for O_i in MgO [12] and sapphire [9], including recent study of the ground state of neutral O_i in $MgAl_2O_4$ [13]; the split interstitial (dumbbell) configuration was confirmed, in agreement with previous classical, pair-potential calculations [14]. One of open questions is, in which charge state O_i migrates in magnesium-aluminium spinel and how the charge state affects its migration energy. As we demonstrated for sapphire [15], migration energy for a charged interstitial oxygen could be considerably smaller than for the neutral one. Thus, the main aim of this study is first principles calculations of the interstitial oxygen migration in different charge states.

2. Computational details and defect model

Magnesium aluminate spinel $MgAl_2O_4$ crystal containing radiation point defects – interstitial oxygen atoms and F centers (O_i or F) have been simulated using linear combination of atomic orbitals method within density functional theory (DFT) approach. To perform spin-polarized calculations, we used CRYSTAL17 computer code [16] for periodic systems using hybrid HSE06 exchange-correlation functional [17]. We have used the all-valence basis sets (BS) of atomic Gaussian type functions (GTFs) both for O atoms (6s-2111sp-1d) [18], as well for Mg atoms (8s-511sp-1d) [19]. Alternatively, for Al atoms, the effective core pseudopotential (ECP) with $3s^2 3p^1 3d^0$ external shell has been used [20].

To avoid defects interaction in a periodic model, supercells of two sizes were used: a conventional cell of 56 atoms (four primitive unit cells) and 2x2x2 supercell (eight primitive unit cells) of 112 atoms. The reciprocal space integration has been performed by sampling the Brillouin zone with the 6x6x6 Monkhorst-Pack mesh

[21] for 56 atom supercell and 4x4x4 for 112 atom supercell. Calculations of point defects were performed using standard geometry optimization and energy minimization procedures [16]. Convergence criteria was set to 10^{-7} a.u. for self-consistency procedure. The effective charges on atoms and bond properties have been evaluated using two different methods: Mulliken population analysis [22] and Hirshfeld-I method [23] as implemented into the CRYSTAL17 code, whereas the bond properties were investigated using TOPOND code [24]. Direct frozen phonon method was used for vibrational frequency calculations [25, 26]. The formation energies for point defects were calculated using the equations:

$$E_{form}^{O_i} = E_{total}^{O_i} - E_{total}^{MgAl_2O_4(perfect)} - 1/2E_{total}^{O_2} \quad (1)$$

$$E_{form}^{Vo} = E_{total}^{Vo} - E_{total}^{MgAl_2O_4(perfect)} + 1/2E_{total}^{O_2} \quad (2)$$

where $E_{total}^{O_i/V_O}$ is the total electronic energy of the spinel supercell containing defect, $E_{total}^{MgAl_2O_4(perfect)}$ - the total electronic energy of a perfect supercell, and $E_{total}^{O_2}$ - the total electronic energy of oxygen molecule.

To estimate migration barriers for oxygen interstitial (O_i) in spinel, we used a distinguished reaction coordinate method [26] as implemented in CRYSTAL17 code. The ground-state dumbbell configuration of O_i defect was the starting point for migration. Simulations of migration paths have been calculated in internal coordinates, where one coordinate (the distance between O_i and selected regular oxygen atom to which it moves) was frozen on each optimization step. Each migration path was calculated using 10-12 configurations. We assume that oxygen vacancy is well-separated from oxygen interstitial, so it does not affect oxygen atom migration. To calculate *charged* oxygen interstitial atom, we used the ground-state configuration of a supercell, containing neutral oxygen interstitial defect, then added one electron to the system and reoptimized the atomic structure. Uniform background charge density neutralized the negative charge in the reference cell [16]. The oxygen F-center was simulated by removing electrons and nuclear charge from oxygen atom site, leaving the basis set centered at the atomic position.

For the crystallographic parameters of $MgAl_2O_4$ we obtained the lattice constant a=8.064 Å and internal coordinate u=0.264 which is in good agreement with experimental values a=8.081 Å and u=0.2623 [27]. The calculated bandgap at the Γ-point is 8.79 eV which only slightly overestimates the experimental value of 7.8 eV [28]. The effective charges calculated by Mulliken analysis (Mg – +1.7*e*, Al – +1.5*e*, O – -1.43*e* are lower than the ones obtained by Hirsfeld-I method (Mg – +2.0*e*, Al – +2.48*e*, O – -1.74*e*. Both methods clearly show that Mg-O bond nature is fully ionic (zero bond population), while Al-O bond is ionic mixed covalent nature. As it was shown for corundum [23], where O-Al electron back-donation is also observed, Mulliken analysis overestimates this effect, which is also present in spinel.

3. Results and discussion

3.1 Formation energies and charges for neutral defects

According to our results obtained for 56 and 112 atom supercells (Table 1), the ground-state configuration for oxygen interstitial in a spinel is the O_i-O_{reg} pair formed by O_i with one of regular oxygen atoms (known also as the *dumbbell* or *split interstitial*), centered at a regular oxygen lattice site. We found similar dumbbell configurations in previous calculations for O_i in MgO [12] and sapphire [29]. But unlike binary oxides, the regular O site is occupied here asymmetrically: one of dumbbell O atoms forms two Al-O bonds, while a second O forms only one Al-O bond and has a stronger ionic interaction with Mg atom. The initially neutral O_i attracts additional electronic density, which results in almost symmetrical charge distribution between the two oxygen atoms in the dumbbell. For better understanding of the dumbbell O_i-O_{reg} properties, we performed vibrational frequency and density of states calculations, as well as used topological analysis of the electron density, according to Quantum Theory of Atoms in Molecules (QTAIM) [30, 31].

Table 1 Neutral defect formation energies, bond length in O_i-O_{reg} pair and O_i effective charge

Supercell	Formation energies, eV	$d_{O\text{-}O}$, Å	Effective charges of O_i and O_{reg}, *e*

E	F-center	O_i		Mulliken	Hirshfield-I
56 atoms	7.88	2.31	1.42	-0.61/-0.65	-0.83/-0.84
112 atoms	7.92	2.45	1.42	-0.63/-0.64	-0.84/-0.83

The defect formation energies are close, ca. 8 eV, in agreement with. The analysis of electronic density reveals a covalent bonding between two oxygen atoms. Total effective charge of O-O dumbbell is lower than effective charge of oxygen atom in perfect spinel, because some charge density is redistributed toward Al atom to form a new bond. The dumbbell contains no unpaired electrons and its ground state is singlet. Mulliken population analysis as well as topological analysis reveal covalent bonding between two oxygen atoms. Plotted 2D Laplacian $\nabla^2\rho$ (Fig. 3) of electron density makes the atomic shell structure visible, which cannot be observed through the topology of ρ. The interatomic distance in the dumbbell of 1.42 Å lies in-between 1.33 Å typical for superoxides O_2^- and 1.49 Å typical for peroxide O_2^{2-} [32] and close to our finding for the dumbbell in sapphire (see also ref. [29] and table 3 therein). The total effective charge of O-O pair found by two methods (-1.26*e*/-1.67*e*) is smaller than could be expected for peroxide species (-2*e*). Lastly, the calculated O-O vibrational frequency of 1142 cm^{-1} is characteristic for superoxide O_2^- ion (1145 cm^{-1} [32]). The possible explanation for reduced charge can be that part of O*2p* electron densities are involved in the Al-O bond formation, and remaining electrons form O-O bond, what results in formation of occupied bonding σ orbital and empty antibonding σ^* orbital, while the *2p*-orbitals, one on each of the two atoms, are not hybridized and maintain an atom-like character. This idea also can be confirmed by density of states (Fig 1), where two occupied levels lie at top of the valence band, and unoccupied σ^* orbital is ~8 eV higher in energy. The NEXAFS measurements of O 1s→σ^* excitation in various peroxides report values about 8.3-8.8 eV for that transition [33].

Adding one electron (and thus making oxygen interstitial negatively charged O_i^-) results in the significant

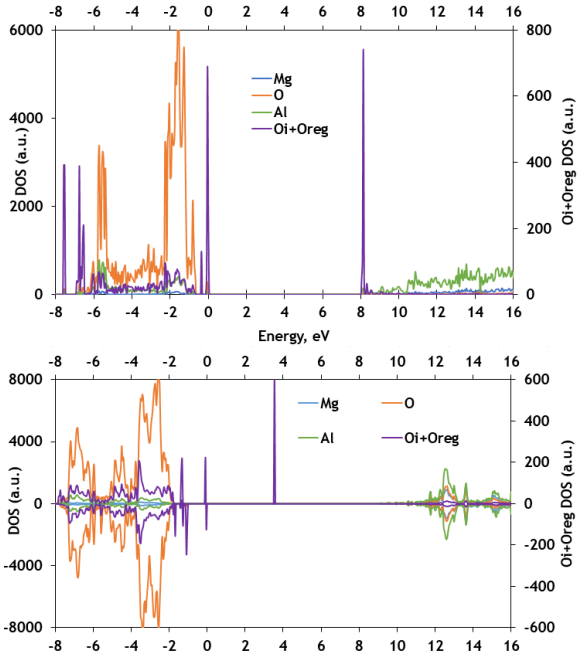

Fig. 1. DOS for a neutral (top) and charged (bottom) oxygen interstitials in spinel. The magnitude of DOS of O-O pair is on right y-axis. Zero energy corresponds to highest occupied energy level.

changes in the O-O pair configuration. The interatomic distance becomes larger by 0.5 Å and increases up to 1.95 Å. The charge and spin density is equally distributed between the two atoms (-1.28 *e* and 0.45μ_B by Hirshfield-I, -0.92 *e* and 0.48μ_B by Mulliken), but vibrational frequencies calculations do not reveal common O-O vibrational mode. All this is similar to the peroxide ions [32] and what we obtained earlier for charged interstitials for sapphire [15]. The Interpretation of DOS in this case becomes more complicated. Additional electron could only occupy σ^* orbital, and that would result in breaking the O-O bond. Performing electron density analysis, we found that weak bonding is still present between two oxygen atoms. Thus, the occupation

of σ^* orbital can be more energetically favourable than other configurations without O-O interactions, as in other oxides oxygen interstitial occupying octahedral or tetrahedral sites is unstable.

3.2 Migration paths of O_i atom in spinel

The difference in defect energies and charges between two used supercells is very small, so the 56 atom model can be considered as a good choice for further modelling single point defects. Still, the larger supercell was used in migration barrier calculations, to avoid possible artifacts.

Three nearest to O_i regular oxygen atoms within 2.55 Å distance were selected as a final destination for oxygen migration, leaving its partner in dumbbell (shown in dotted line) and moving to another regular oxygen ion. The migration paths and the calculated energy curves are shown in Fig.2. All of them reveal a clear energy barrier and end up with the formation of a new O-O pair with regular oxygen atom. Estimated barriers lie in the range from 1 eV to 2.4 eV. For more detailed analysis, let us take a closer look on surroundings of O_i and the electron density distribution in starting/final point (considered as equivalent) and the top of barrier.

The two paths, I and II, with low energy barrier have practically identical saddle points. Along the paths O_i attracts electron density from O_{reg2} atom, while O_{reg1} lets its normal charge in perfect crystal (-1.47*e*). At the

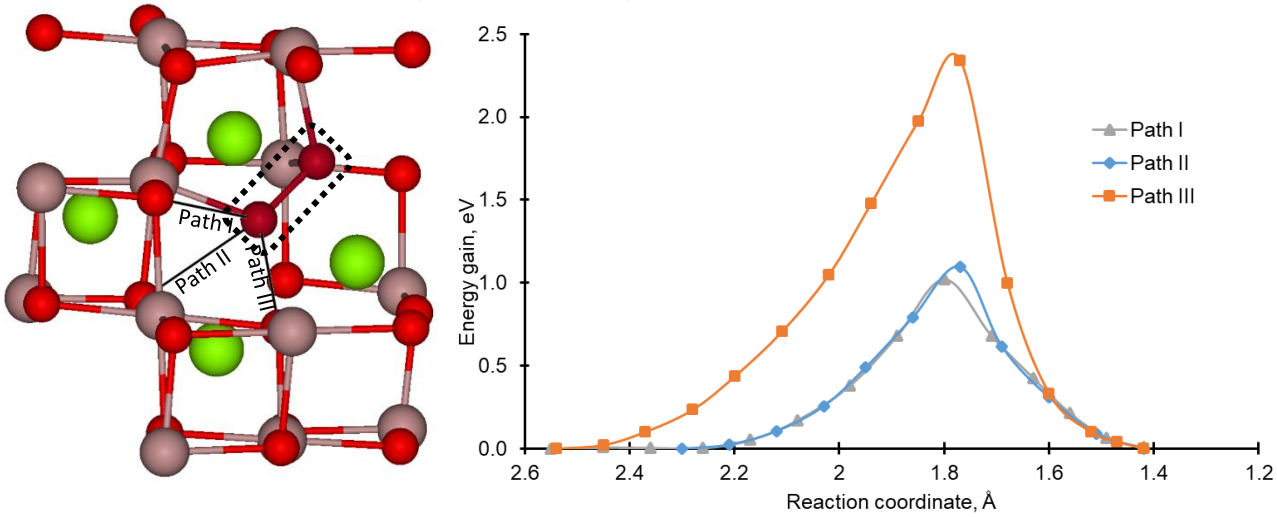

Fig. 2. Left: fragment of 113 atom supercell with three migration paths of neutral O_i in spinel crystal. Green balls correspond to Mg atoms, grey-brown – Al atoms, and red – O atoms. The dumbbell (O-O pair) is shown in dark red and highlighted with dotted rectangle. Right: the energy curves for three migration paths of neutral O_i with d energy barriers. The reaction coordinate is the distance between end atom of a dumbbell and a regular O ion to which it moves

saddle point O_i attracts 0.5*e* in total, almost equally from both oxygen atoms. A closer look on the saddle point of path III clearly shows that the rise in energy barrier arises due to a strong interaction with Mg atom. At the same time, O-O bond lengths and populations are very similar to paths I and II, the only difference is interaction with Mg atom instead of Al atom. This observation is especially important for Mg-rich spinels, where antisite defects Mg_{Al} are common, which could affect oxygen migration. Also, in absence of strong Al-O interaction, Mulliken and Hirshfeld-I methods give similar results for O_i effective charge. Migration barriers of ~1 eV are smaller than calculated for neutral oxygen interstitials in corundum (~1.3 eV) and MgO (1.45 eV). The reason for that could be in asymmetrical surrounding of the O-O dumbbell in spinel.

Table 2. Configuration of neutral O_i and its surrounding at the top of migration barrier

Trajectory		I	II	III
Energy barrier, eV		1.0	1.1	2.4
O_i charge, *e*	Mulliken	-0.57	-0.56	-0.55
	Hirshfeld-I	-0.71	-0.71	-0.56

NN distance, Å	O_{reg1} 1.66 Å, Al 1.78 Å, O_{reg2} 1.79 Å, Mg 2.07 Å	O_{reg1} 1.72 Å, O_{reg2} 1.77 Å, Al 1.77 Å, Mg 2.08 Å	O_{reg1} 1.63 Å, O_{reg3} 1.77 Å, Mg 1.86 Å, Al 2.33
Bond population of O_i with NN	-0.11, 0.30, -0.28, 0.04	-0.10, -0.24, 0.31, 0.04	-0.09, -0.28, 0.06, 0.04

3.3 Migration paths of O^-_i ion in spinel

In contrast with a neutral O_i, *charged* interstitial oxygen O_i^- in spinel forms dumbbell which symmetrically occupies a regular oxygen site: each of two oxygen atoms forms the covalent bonds with 2 Al atoms and one ionic bond with Mg atom. Within 1NN oxygen atoms, there exist two symmetrically inequivalent migration paths for interstitial. As was mentioned previously, charged oxygen interstitial has a weaker O-O bond, what also can be seen on the Laplacian of electron density maps (Figs. 4 and 5).

Calculated migration path I shows smaller (~0.8 eV) energy barrier than for neutral O_i. Surrounding of oxygen interstitial in a top of migration barrier also differs comparing to neutral one: there O_i has broken one of two bonds with Al, weak interaction with O_{reg1}, and, to compensate negative charge, it makes additional ionic with one more Mg atom. As a result, path is curved that way, so it goes through middle point between two Mg atoms. This observation could be important when studying antisite defect effects on interstitial mobility in spinel.

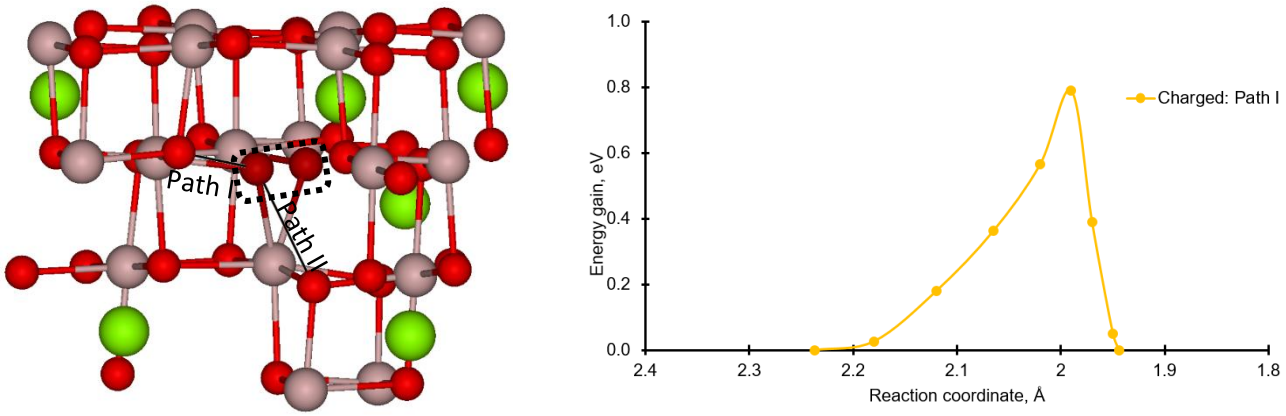

Fig. 4. Left: fragment of 113 atom supercell with two migration paths of charged O_i in spinel crystal. O-O pair atoms shown in dark red and highlighted with dotted rectangle. Right: Energy curves for migration paths of charged O_i with estimated energy barriers.

Table 3. Configuration of neutral O_i and its surrounding at the top of migration barrier

Trajectory		I	II
Energy barrier, eV		0.8	
O_i charge, *e*	Mulliken	-0.57	
	Hirshfield-I		
NN distance, Å		Al 1.76 Å, Mg 1.91 Å, O_{reg1} 1.99 Å O_{reg0} 2.21 Å	
Bond population of O_i with NN		0.34, 0.06, -0.12, -0.06	

Path II

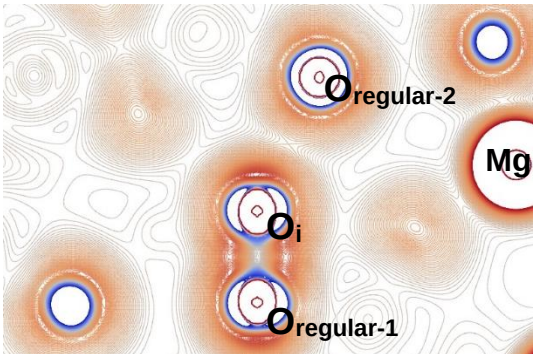

Path III

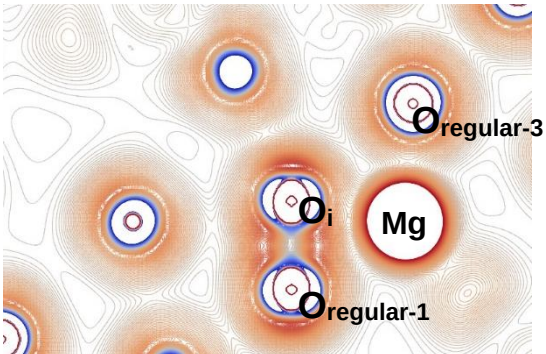

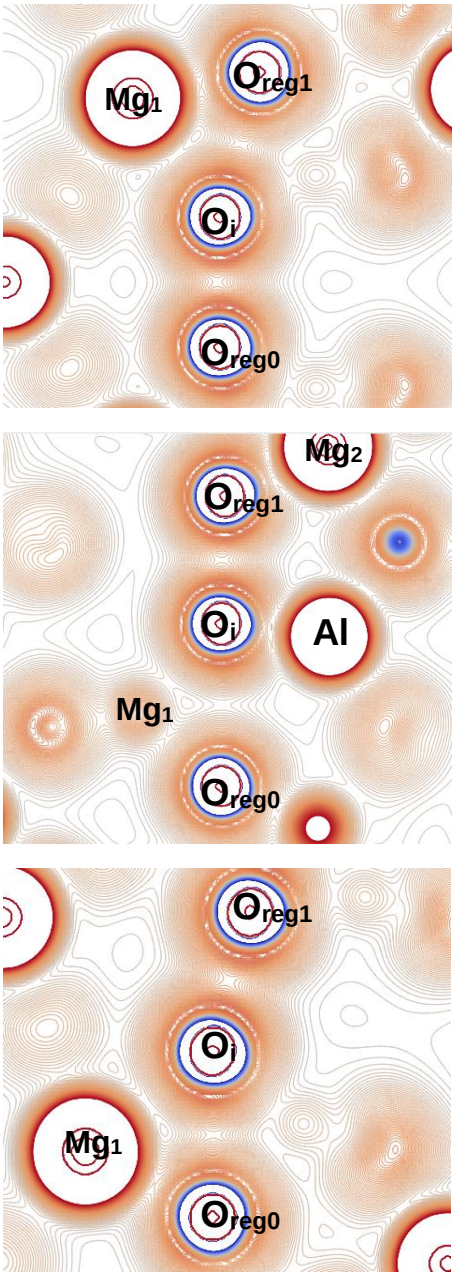

Fig. 5. 2D plot of Laplacian of electron density ($\nabla^2\rho$) of defective spinel. Charged interstitial configurations in starting point (top), in top of energy barrier (middle) and final point (bottom) are shown. All mapped planes are build through O_{reg0} – O_i – O_{reg1} points.

4 CONCLUSIONS

Xxxx

Acknowledgments

This study has been carried out within the framework of the EURO fusion Consortium and has been provided funding from the Euratom research and training program 2014–2018 under grant agreement No. 633053. The authors are indebted to A.I. Popov, A.C. Lushchik and R. Vila for stimulating discussions. Technical assistance from O. Lisovski is appreciated too. The views and opinions expressed herein do not necessarily reflect those

of the European Commission. Calculations have been performed using Marconi supercomputer system based in Italy at CINECA Supercomputing Centre.

References

[1] A. Ibarra, E.R. Hodgson, Nucl. Inst. Meth. B **218** (2004) 29.

[2] F. Mota, C.J. Ortiz, R. Vila, N. Casal, A. Garcia, A. Ibarra, J. Nucl. Mater. **442** (suppl. 1) (2013) 5699

[3] A. Lushchik, S. Dolgov, E. Feldbach, R. Pareja, A.I. Popov, E. Shablonin, V. Seeman, Nucl. Inst. Meth. B xxx, (2018) xx.

[4] D. Bacorisen, R. Smith, B.P. Uberuaga, K.E: Sikafus, Phys. Rev. B **74** (2006) 214105

[5] P.B. Uberuaga, M. Tang, C. Jiang, J.A. Valdez, R. Smith, Y. Wang, K.E. Sikafus, Nat. Comm. **6** (2015) 8750

[6] A. Lushchik, Ch. Lushchik, K. Schwartz, E. Vasil'chenko, T. Karner, I. Kudryavtseva, V. Issakhanyan, A. Shugai, Nucl. Inst. Meth. B **266** (2008) 2868.

[7] A.I. Popov kotomin kuzovkov Fiz. Nizkih temp. 2017

[8] E.A. Kotomin, A.I. Popov, Nucl. Inst. Meth. B **141** (1998) 1.

[9] E.A. Kotomin, V.N. Kuzovkov, A.I. Popov, R. Vila, Nucl. Inst. Meth. B **374** (2016) 107.

[10] J-M. Costantini, G. Leiong, M. Guillaumet, W.J. Weber, S. Takaki, K. Yasuda, J. Phys. Cond. Matt. **28** (2016) 325901.

[11] S. Jiang, T. Lu, Y.I. Long, J. Chen, J. Appl. Phys. **111** (2012) 043516

[12] T. Brudevoll, E.A. Kotomin, N.E. Christensen, Phys. Rev. B **53** (1996) 7731–7735

[13] R.A. Evarestov, A. Platonenko, Yu.F. Zhukovskii, J. Comp. Mat. (2018)

[14] C.A. Gilbert, R. Smith, S.D. kenny, S.T. Murphy, R.W. Grimes, J.A. Ball, J Phys. Cond. Matt. **17** (2009) 275406

[15] A. Platonenko, D. Gryaznov, Yu. F. Zhukovskii, E.A. Kotomin, Nucl. Inst. Meth. B **xx** (2018)

[16] R. Dovesi, V. R. Saunders, C. Roetti, R. Orlando, C. M. Zicovich-Wilson, F. Pascale, B. Civalleri, K. Doll, N. M. Harrison, I. J. Bush, P. D'Arco, M. Llunell, M. Causà, Y. Noël, L. Maschio, A. Erba, M. Rerat, S. Casassa CRYSTAL17, (2017) CRYSTAL17 User's Manual. University of Torino, Torino.

[17] A. V. Krukau, O. A. Vydrov, A. F. Izmaylov, G. E. Scuseria, J. Chem. Phys. **125** (2006) 224106

[18] J. Baima, A. Erba, M. Rérat, R. Orlando, R. Dovesi, J. Phys. Chem. C **117** (2013) 12864–12872

[19] M.I. McCarthy, N.M. Harrison, Phys. Rev. B **49** (1994) 8574–8582

[20] M. Causà, R. Dovesi, C. Roetti, Phys. Rev. B **43** (1991) 11937–11943

[21] H.J. Monkhorst, J.D. Pack, Phys. Rev. B. **13** (1976) 5188–5192

[22] R.S. Mulliken, I. J. Chem. Phys. **23** (1955) 1833–1840

[23] C. M. Zicovich-Wilson, M. Hô, A. M. Navarrete-López, S. Casassa, Theor. Chem. Acc. 135 (2016) 188

[24] C. Gatti, Zeitschrift fur Kristallographie **220** (2005) 399

[25] F. Pascale, C.M. Zicovich-Wilson, F. Lopez Gejo, B. Civalleri, R. Orlando, R. Dovesi, J. Comput. Chem. **25** (2004) 888–897

[26] C.M. Zicovich-Wilson, F. Pascale, C. Roetti, V.R. Saunders, R. Orlando, R. Dovesi, J. Comput. Chem. **25** (2004) 1873–1881

[27] M. Ishii, J. Hiraishi, T. Yamanaka, Phys. Chem. Minerals. **8** (1982) 64–68

[28] M.L. Bortz, R.H. French, D.J. Jones, R.V. Kasowski, F.S. Ohuchi, Phys. Scr. **41** (1990) 537–541

[29] R.A. Evarestov, A. Platonenko, D. Gryaznov, Yu.F. Zhukovskii, E.A. kotomin, Phys Chem Chem Phys **19** (2017) 25245.

[30] R. F. W. Bader, Atoms in Molecules - A Quantum Theory, vol. 22 of International Series of Monographs in Chemistry. Oxford, UK: Oxford University Press (1990)

[31] C. Gatti, V. R. Saunders, C. Roetti, J. Chem. Phys. **101** (1994) 10686–10696

[32] E. Wiberg, N. Wiberg, A.F. Holleman, Inorganic Chemistry, Acad. Press, San Diego, 1st English edn, 2001, p. 1884.

[33] E. Rühl, A.P. Hitchcock, Chem. Phys. **154** (1991) 323-329

Institute of Solid State Physics, University of Latvia as the Center of Excellence has received funding from the European Union's Horizon 2020 Framework Programme H2020-WIDESPREAD-01-2016-2017-TeamingPhase2 under grant agreement No. 739508, project CAMART²